CAMBRIDGE
UNIVERSITY PRESS

RESEARCH ARTICLE

Porcospino, spined single-track mobile robot for inspection of narrow spaces

Shahab E. Nodehi, Luca Bruzzone and Pietro Fanghella

Department of Mechanical, Energy, Management and Transport Engineering (DIME), University of Genoa, Genoa, Italy
Corresponding author: Luca Bruzzone; Email: luca.bruzzone@unige.it

Abstract

This paper discusses the design and the experimental tests on Porcospino, a bio-inspired single-track mobile robot for inspection of unstructured environments characterized by narrow spaces. It is an evolution of SnakeTrack, a single-track robot with steering capabilities; differently from SnakeTrack, the track modules of Porcospino are characterized by elastic spines, which improve traction on uneven and irregular terrains. The main body is a vertebral column, comprising a series of vertebrae connected by compliant joints and two end modules. Each end module carries two sprockets, sharing a common actuator, to drive the single peripherical track. Moreover, each end module hosts an actuator for track steering. The remaining mobilities of the vertebral column allow it to cope passively with the terrain profile, to enhance traction. The control unit, batteries, drivers, and environmental sensors are placed along the vertebral column. Both the end modules are equipped with a camera for intermittent vision, which is possible thanks to openings realized on the track modules. The experimental campaign on the first Porcospino prototype is discussed, highlighting the differences with its earlier version.

1. Introduction

Nowadays, service robotics is one of the fastest-growing research fields. In particular, ground mobile robots (GMRs) can reduce the risks of death or injuries, replacing the human presence for surveillance and inspection in many harmful and insecure environments, for example, in case of chemical or radioactive pollution, in dangerous salvage tasks, or in homeland security operations.

GMRs can be profitably applied in many types of calamities, such as floods, hurricanes, earthquakes, and fires. In these situations, it is essential to reach the casualties as soon as possible. Consequently, many research efforts are devoted to the development of search and rescue robots, capable of aiding the personnel by gathering data from the disaster site.

Independently of the carried equipment, GMRs can be classified according to their type of locomotion, and the selection of the locomotion system is the starting point of the design of GMRs for operation in unstructured environments. There are three main classes of GMRs: legged [1, 2] (L), wheeled [3, 4] (W), and tracked robots [5, 6] (T). These three locomotion principles can be mixed, giving rise to the hybrid combinations proposed in the scientific literature: LT [7, 8], WT [9, 10], LW [11, 12], and LWT [13]. The functional features of these hybrid robots are discussed and compared in ref. [14].

An interesting solution for inspection of environments characterized by narrow spaces is to combine tracked modules in series: examples are the snake-like robot with active flippers for urban search and rescue tasks proposed in ref. [15], and the amphibious robot discussed in ref. [16], capable of swimming by swing motion, besides moving on uneven ground. These robots are long and thin and have the advantages of tracked locomotion. Tracked robots [17] are particularly suitable for uneven and yielding grounds, thanks to their large contact surface with the terrain. On the other hand, their speed and efficiency are lower with respect to wheeled ones.
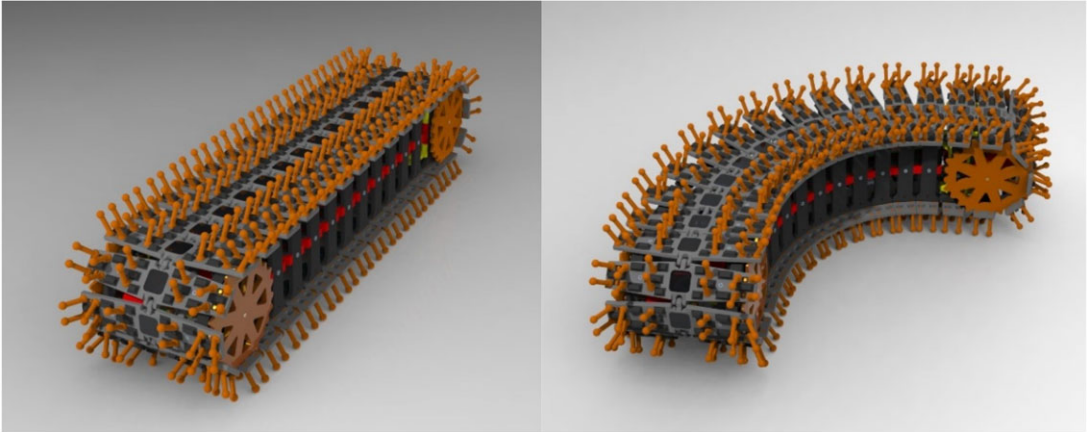
Figure 1. *External view of Porcospino: straight position (left) and steering position with minimum turning radius (right).*

An alternative approach to design long and thin tracked robots suitable to move in narrow spaces is to equip a worm robot with a peripheral track. Examples are the Flexible Mono-Tread Mobile Track (FMT) [18, 19] and the Reconfigurable Continuous Track Robot (RCTR) [20].

In this paper, a novel single-track robot with steering capability, Porcospino, is proposed and discussed. It represents the evolution of the SnakeTrack robot [21], with elastic spines mounted on the track modules to improve traction and shock adsorption. Moreover, with respect to ref. [21], the relation between the angular displacement of the robot vertebral column and the turning radius is described. The remaining of the paper is organized as follows: Section 2 outlines the functional design of the proposed robot; Section 3 compares Porcospino to other GMRs with single peripheral track; Section 4 is focused on the embodiment design of the vertebral joints; Section 5 discusses the kinematics of the underactuated steering; Section 6 presents the experimental campaign; and Section 7 debates conclusions and future developments.

2. Functional design of Porcospino

Figure 1 shows the CAD model of the Porcospino robot, characterized by a length of 670 mm, a width of 165 mm, and a height of 145 mm. Its mechanical architecture is composed of a vertebral column and of a peripheral track, in relative motion. Both the column and the track are deformable, to allow steering and to cope with the ground unevenness.

The vertebral column of Porcospino (Fig. 2) is characterized by 10 vertebrae (V) and 2 end modules (E). The robot is modular, so its length can be varied by adopting a different number of vertebrae and track modules. The vertebrae are connected by compliant joints, which are designed with low rotational stiffness around the yaw axis in order to reduce energy consumption while steering (Fig. 1, right).

Porcospino is externally and functionally symmetric with respect to all the three middle planes, so it is fully operative after inverting locomotion direction or after a capsize. Each end module hosts two actuators. The first actuator (TA, Fig. 2) is a brushed DC motor with reduction gearbox, which drives the two track sprockets (TS), connected to a common axis, through a couple of gears (TG).

The second actuator (SA, Fig. 2) is a gearmotor connected to a winch, which drives the lateral flexion by pulling a 1 mm dyneema rope (R). There are two ropes, one for each side of the robot, guided along the flank of the column by lateral holes of the vertebrae (H, Fig. 3) and pulled by the two SA actuators. Lateral steering is realized by pulling one rope and releasing the other one at the same time. As a consequence, the motions of the two SA actuators must be properly coordinated; when one SA actuator
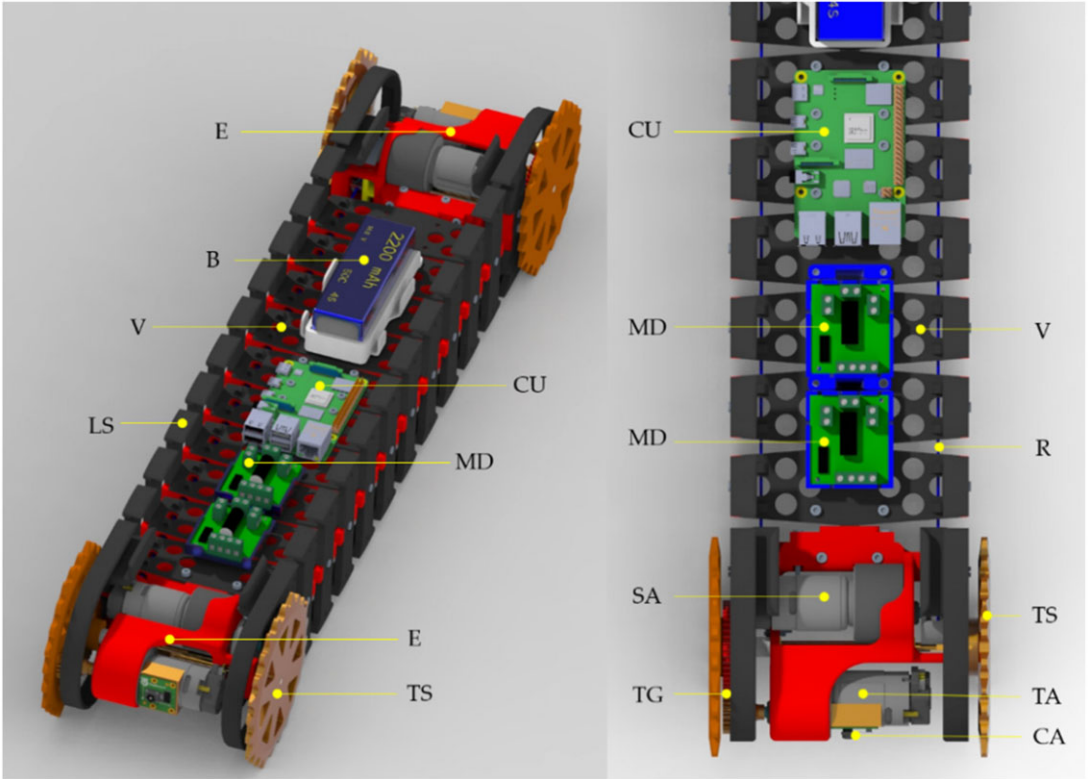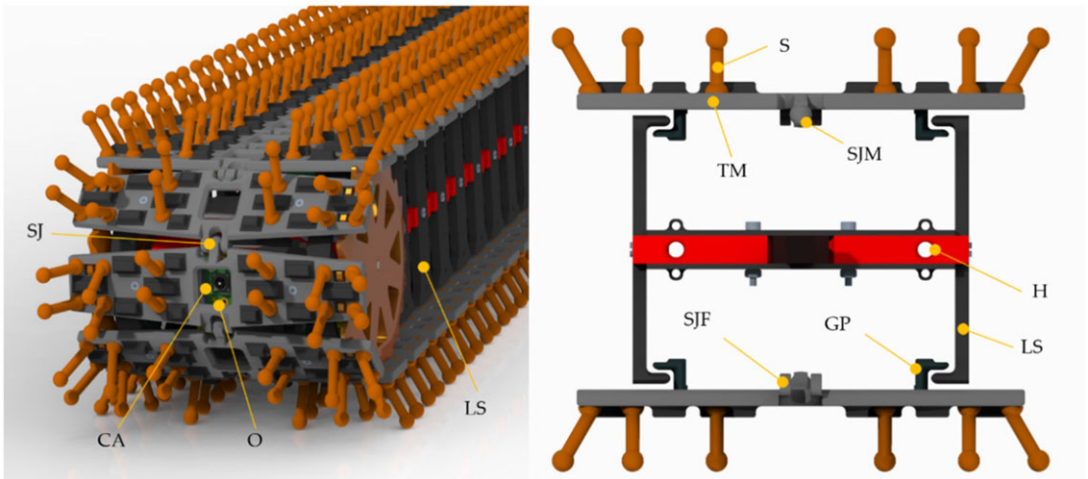
Figure 2. *Vertebral column of Porcospino.*

Figure 3. *Detail of the track modules: opening for vision (O, left); transversal section of the track guidance system (right).*

pulls a rope, the other SA actuator must loosen the opposite rope, as it will be discussed in Section 5. Also the motions of the two TA actuators are not independent, since all the sprockets actuate the same track with the same tangential speed.

Figure 3 shows a detailed view of the track modules (TM, Fig. 3). Two cameras (CA, Figs. 2 and 3) are mounted on the end modules. Their vision is not continuous but intermittent, through the central openings of the track modules (O, Fig. 3). Each vertebra is equipped with lateral supports (LS, Fig. 3), which guide the track by their contact with the guiding pegs of the track modules (GP, Fig. 3). The track modules are connected by spherical joints (SJ, Fig. 3), composed of a male part (SJM) and a female part (SJF), printed directly on the tracked module. The two parts of the spherical joint can be assembled, thanks to the elasticity of the female part. On the contrary, the track spines (S, Fig. 3) and the guiding pegs of the track modules (GP, Fig. 3) are printed separately and then assembled by interference fit.

The spines have been designed to reach a satisfying compromise between the capability of gripping obstacles and terrain irregularities and shock absorption. The spines are realized in ABS; they have a length of 25 mm, a diameter of 5 mm, and spherical ends with 8 mm diameter. As it can be observed in Fig. 3 (left), all the rows of spines are inclined at 30° with respect to the normal to the track surface; this inclination assures better shock absorption, since the spines can bend more easily when the track bumps the ground or an obstacle.

Since the track moves, camera vision is possible only when the cameras CA are aligned with the track openings O. However, this is not a remarkable limitation for usual inspection tasks: the nominal robot speed is 0.1 m/s, and the pitch of the track modules is 40 mm; consequently, the frame rate when the robot travels at nominal speed is 2.5 FPS. Even if this frame rate is not adequate for a fluid vision, it is sufficient to pilot the robot, considering its relatively low speed. Moreover, the robot can stop with alignment between cameras and openings when it is necessary to monitor with continuous vision at high frame rate.

Besides performing its structural function, the vertebral column hosts the control unit (CU, Fig. 2), the batteries (B), and the motor drivers (MD). Moreover, other exteroceptive sensors, besides the two cameras, can be selected for the specific operative needs [22–25] and mounted along the vertebral column in the empty room delimited by the track modules (TM) and by the lateral supports (LS). Thanks to the robot modularity, length and room for the payload can be varied based on task requirements. For example, the robot can be equipped with thermal, radioactivity, and chemical exteroceptive sensors, and with proprioceptive ones like inertial measurement units (IMUs) and encoders to measure the deformation of the vertebral column, as an aid for motion planning.

In the first prototype, no exteroceptive sensor is mounted on board except the two cameras (Raspberry Pi Camera Module 2), and the only installed proprioceptive sensors are the motor encoders (Micromotors Rh158). The first tests are focused mainly on the functionality, performance, and reliability of the locomotion system; consequently, the motor encoders are not used for navigation purposes: the operator guides the robot motion by means of an RC control unit (Futaba T6K-V3S) by using two analog channels. One RC channel commands in parallel the two TA actuators through the motor driver Sabretooth 2×5. The second RC channel drives in parallel the SA actuators in opposite directions (one pulls, one releases, as previously discussed) through the same motor driver. In a future layout, a Raspberry PI 4 Model B 8 Gb RAM controller will be used to realize an automatic guidance system with on-board computational capabilities.

3. Comparison with other mobile robots with single peripheral track

In case of earthquakes or other disasters involving collapsed buildings, robots can be useful for search operations. Moreover, in some calamities, robots can monitor the presence of chemical or radioactive pollution without direct human intervention. Such robots must be capable of traveling across the rubble and accessing the interior of debris piles, moving in narrow spaces. To face these challenges, serpentine and snake-like robots have been proposed [15, 16]. The main advantage of these architectures is that the ratio between the length and the front section is high, so the robots can navigate in

Table I. *Comparison of ground mobile robots with single peripheral track.*

	FMT	RCTR	ST	PS
Lateral flexion of the vertebral column (steering)	Actuated by toothed belts	Not possible with a single module	Actuated by ropes	Actuated by ropes
Retroflexion of the vertebral column	Actuated by toothed belts	Actuated by a locking mechanism	Passive	Passive
Torsion of the vertebral column	Passive	Not allowed	Passive	Passive
Bidirectional motion	Yes	No	Yes	Yes
Bilateral guidance of the tracks along the vertebral column	Yes	No	No	Yes
Number of actuators for track propulsion	1 (on one end module)	2 (one on each end module)	2 (one on each end module)	2 (one on each end module)
Shock absorption	Low	Very low	Low	High
Possibility of recovery after a capsize on a flank	Yes	No	Yes	Yes
Camera vision	No	No	Front and rear	Front and rear
Installation of payload along the vertebral column	Difficult	Easy	Easy	Easy

Flexible Mono-Tread Mobile Track (FMT) [18, 19], Reconfigurable Continuous Track Robot (RCTR) [20], SnakeTrack (ST) [21], and Porcospino (PS).

narrow spaces while carrying environmental sensors along their body. Moreover, if they are symmetric and bidirectional, they can be fully operative after a 180° capsize, differently from most tracked robots.

Robots with single peripheral track are a subset of the category of snake-like and serpentine robots; since the top and bottom surfaces are completely covered by the track, their motricity is better, and the risk of unwanted contacts of the robot body with the ground, which can lock the robot itself, is lower.

As already said, the concept of single peripheral track robot has been already proposed in [18–21]; Table I summarizes the differences among Porcospino (PS) and the other single peripheral track robots present in the scientific literature: the FMT [18, 19], the RCTR [20], and the SnakeTrack (ST) [21].

The main difference between the four robots is the mobility of the vertebral column. All the robots except the RCTR can bend the vertebral column in the horizontal plane (lateral flexion) for steering; in the FMT, this mobility is driven by a toothed belt, while in ST and PS it is driven by a pair of ropes, for more compactness and to save internal space. The RCTR cannot steer, since this prototype has been developed mainly to study the retroflexion mechanism; the possibility of steering can be obtained by using two tracks in parallel or in series [20], but in this case the robot cannot be considered a single peripheral track robot. The active lateral flexion of FMT, ST, and PS can also be used to recover from a 90° capsize on a flank, as it will be discussed in Section 6.

As regards the retroflexion, it is actuated by a toothed belt for the FMT, while in the RCTR it is obtained by means of a mechanism, placed on the front wheel, that locks the relative rotation of the adjacent track modules, while the releasing mechanism is on the rear wheel. This solution allows retroflexion but has drawbacks; the robot is not bidirectional, differently from the others, and the track has a low resistance to shocks due to its complex construction with rotating locking pins. The ST and PS robots, differently from FMT and RCTR, have only passive retroflexion, induced by the contact with the ground profile, and this limits the capability of facing higher obstacles. However, the introduction of the elastic spines in PS has improved its capability of facing square steps, as it will be discussed in Section 6.

As regards the torsion of the vertebral column, which enhances the capability of coping the ground unevenness, it is passive for the FMT, ST, and PS robots, and it is not allowed for the RCTR robot due to the design of the track modules.

Another important feature is the type of guidance of the track along the vertebral column. In the RCTR and ST robots, the track is guided laterally, but it can depart from the vertebral column if the contact forces with the ground are not properly distributed. In the PS robot, differently from the ST, the lateral support and the guiding pegs (LS and GP, Fig. 3) have been designed to bilaterally guide the track in all directions, as it occurs for the FMT.

In the PS robot, the track propulsion is performed by two actuators (TA, Fig. 2), placed on the two end modules, similarly to ST and RCTR. On the contrary, the track propulsion in the FMT robot is performed by only one motor and only one pair of sprockets is actuated, while the other pair is idler. The solution with two actuators for track propulsion is preferable for two reasons. First, with only one track actuator, the robot is not symmetrical and bidirectional from a functional point of view; as a matter of fact, when the robot climbs a slope, the distribution of the forces along the track and the robot dynamic behavior are different if the actuated end module is placed on the front end module or on the rear end module. Moreover, if all the sprockets are actuated, the propulsive force is distributed more evenly along the track itself, and this reduces the maximum tension along the track, thus improving the reliability of the track guidance.

The main difference between the PS and ST robots is the introduction of the elastic spines, which enhance the capability of adapting to the ground, thus improving traction, and provide shock absorption. The effectiveness of the elastic spines is discussed in Section 6.

An advantage of the ST and PS robots over the other two is the possibility of placing front and rear cameras on the end modules, thanks to the track design. Moreover, similar to RCTR, there is room for installing payload along the vertebral column.

Overall, the comparison summarized in Table I shows that the PS robot has the most complete features, except than the active retroflexion of the vertebral column, which is useful to lift the front of the track in order to overcome higher obstacles. This feature will be implemented in future versions by adopting a system similar to the one used for lateral flexion, with two additional ropes along the vertebral column and two additional actuators hosted in the end modules.

4. Embodiment design of the vertebral joints

The vertebral joints must allow spherical relative mobility between two adjacent vertebras. While the spherical joints of the tracks can have no elastic return force since the tracks follow the path imposed by the vertebral column, the spherical joints of the vertebral column must have an elastic return force (compliant joints) in order to obtain a uniform bending of the vertebral column itself while steering. Moreover, a certain elasticity of the column allows a passive adaptation of the track to the terrain shape, improving traction.

Consequently, the design of the compliant vertebral joints starts from the functional requirements of limited yaw stiffness, for reducing the energy necessary for steering with lateral flexion of the column, and higher pitch and roll stiffnesses, to limit adequately the passive retroflexion and torsion of the column in presence of ground unevenness.

Several alternative realizations of the vertebral joints have been considered. In robotics and mechatronics, compliant joints are often realized by adopting lumped elasticity. A review of the possible designs of compliant universal joints is outlined in ref. [26]. Two significant examples are represented in Fig. 4a and 4b. Besides the pitch (y) and yaw (z) compliances, such universal joints have also a limited roll compliance (x). The two-axis flexure joint shown in Fig. 4a extends to two axes the concept of the classical flexure hinge for revolute joints. It is possible to regulate independently the y and z stiffnesses by varying the two sides of the central rectangular section. In this type of joint, the stress is mainly concentrated close to the central section, penalizing the mechanical resistance, in particular in the case of fatigue stress.
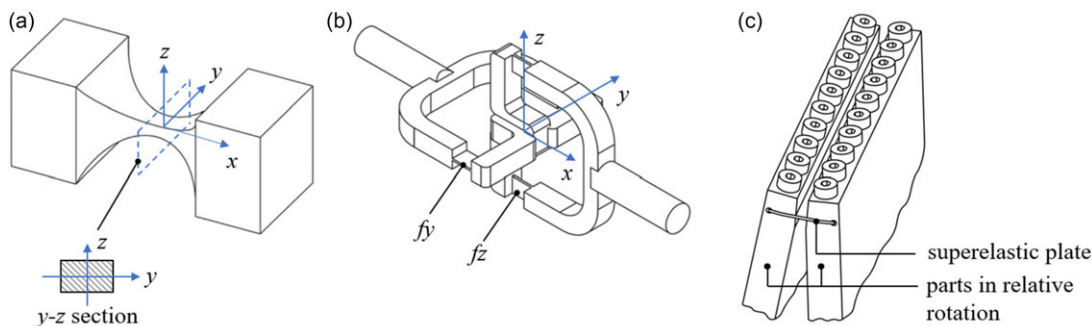
Figure 4. *Compliant universal joints realizations (a, b); revolute joint with superelastic plate (c).*
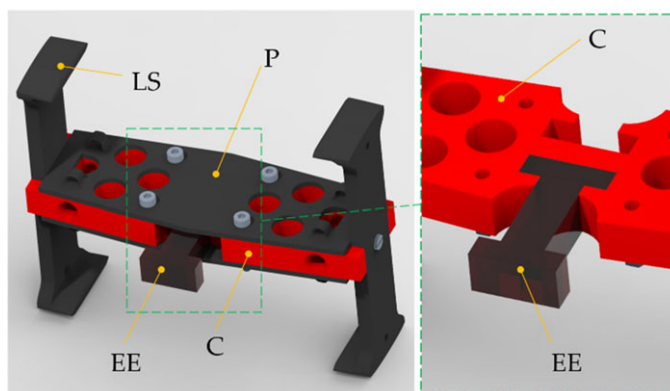

Figure 5. *Constructive design of the vertebral joints with TPU elastic element (EE).*

The compliant universal joint of Fig. 4b partially solves this problem, since the strain is distributed along the plates *fy* and *fz*, with constant thickness. Also for this joint, it is possible to realize different *y* and *z* stiffnesses, by choosing different widths and thicknesses for the two couples of flexure plates. However, the construction of a compliant universal joint in a single part is rather complex and can be faced only by additive manufacturing, with consequent limitations on material properties.

To solve this problem, a possible solution is to realize the flexure plates by means of inserts in superelastic materials (Fig. 4c), as proposed in refs. [27, 28]. Nevertheless, this approach increases size and weight of the joint, since it is necessary to introduce junctions. 3-DoF compliant joints can be realized also through beam-based compliant mechanisms [29], but they are not suitable for the present application for their encumbrance.

To face these issues, an alternative methodology is the soft robotic paradigm; a compliant element is realized not with lumped compliance but with distributed compliance, exploiting the hyperelasticity of the material. A widely used hyperelastic material, suitable for additive manufacturing, is thermoplastic polyurethane (TPU).

Following this approach, the design of Fig. 5 has been obtained. The compliant vertebral joints are realized by TPU elastic elements (EE), locked to the vertebral core (C) by the plates (P); finally, plates and core are connected by bolts. When the elastic element EE is undeformed, there is a small gap $\epsilon = 0.15$ mm between the profiles of the plates P of two adjacent vertebrae (Fig. 6). This gap is obtained by rounding the edges of the plates P (the roundings are represented in red in Fig. 6).

The contact between the plates of two adjacent vertebrae limits the relative pitch motion, and consequently the passive retroflexion of the vertebral column, while the lateral flexion (yaw rotation) is
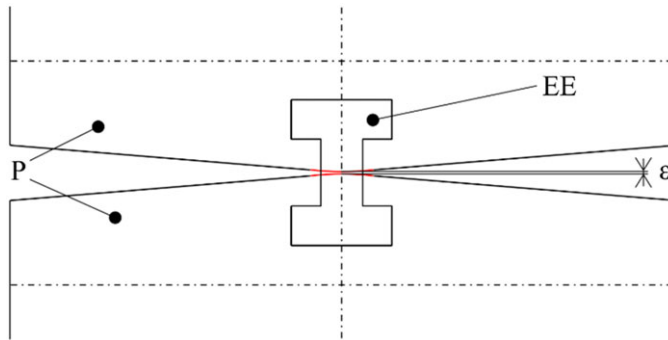
Figure 6. *Profile of the external plates P, with a small gap ε to regulate the passive retroflexion.*

almost not affected by the contact of the plates P. This design of the compliant joints has the following advantages:

- low cost;
- simplification of the geometrical design of the vertebral joints;
- much higher resilience to shocks with respect to conventional compliant joints;
- easy tuning of the maximum amplitude of the retroflexion by varying the gap ε between the plates of adjacent vertebrae.

5. Kinematics of the underactuated steering

The steering system of Porcospino is highly underactuated; as a matter of fact, the lateral flexion of the whole vertebral column is driven by the tension of a single rope, but the vertebral column is characterized by several compliant joints.

Consequently, the definition of the time-varying profile of the column, even with the hypothesis of the robot lying on a flat surface, is a complex problem, which involves the friction conditions between each track module and the ground. In case of uneven terrain, the problem is even more complex, not planar, and not only yaw rotations of the compliant joints, but also their pitch and roll rotations must be considered.

Nevertheless, some useful kinematic relationships can be obtained considering the following assumptions (Fig. 7):

- the robot stands on a flat horizontal surface (planar problem);
- the gap between the plates (Fig. 6) is neglected, and the compliant joint is considered as a pure revolute joint placed in the geometric center of the undeformed elastic element EE;
- the yaw rotation is equal (σ) for all the joints.

The third assumption is a reasonable approximation on flat and uniform surfaces, since the elastic return forces of the compliant joints tend to distribute uniformly the curvature along the vertebral column; this fact is confirmed by the experimental results (Section 6).

Figure 7 represents the geometry of the vertebral column in undeformed (left) and steered position (right). In the figure, three vertebrae are represented, but in general the number of vertebrae is n.

In the steered position, the length of the rope on the external side of the curve (l_{ext}) is represented by the broken line from A_{em} to D_{em}, plus a constant c_r which depends on the geometry of the end modules and the attachment of the rope on the winch.

The length of the rope on the internal side of the curve (l_{int}) is represented by the broken line from B_{em} to C_{em}, plus c_r.
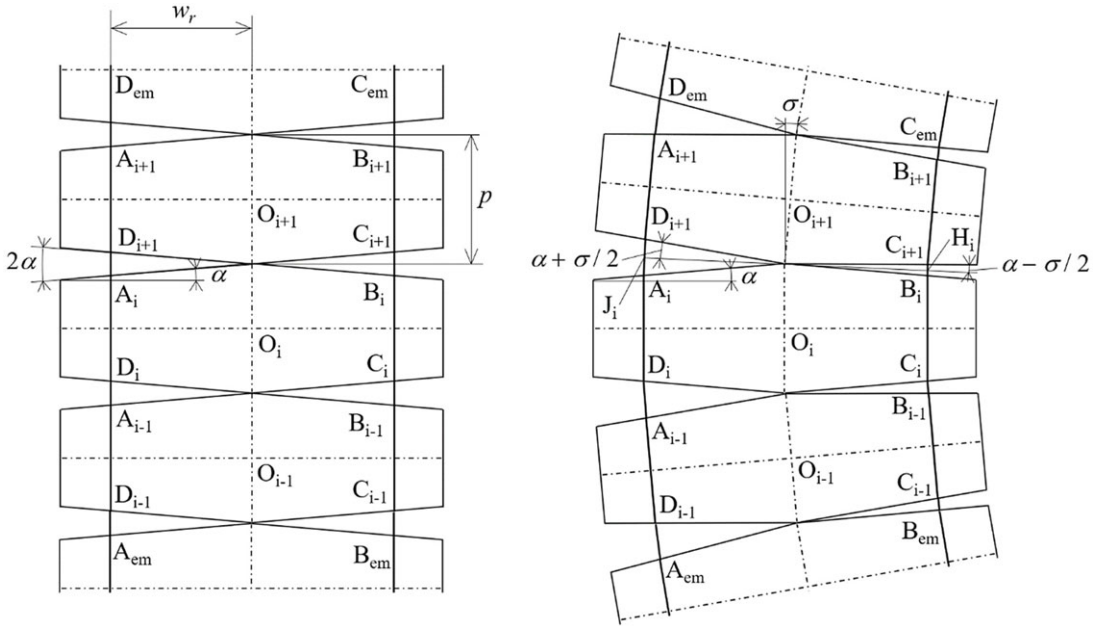
Figure 7. *Relative orientations of adjacent vertebrae in straight position (left) and steered position (right) of the vertebral column.*

Considering the geometry of Fig. 7, it is possible to obtain the following relationships:

$$\overline{A_iD_{i+1}} = 2\overline{J_iD_{i+1}} = 2\frac{w_r}{\cos\alpha}\sin\left(\alpha + \frac{\sigma}{2}\right) \tag{1}$$

$$\overline{B_iC_{i+1}} = 2\overline{H_iC_{i+1}} = 2\frac{w_r}{\cos\alpha}\sin\left(\alpha - \frac{\sigma}{2}\right) \tag{2}$$

$$\overline{A_iD_i} = p - 2w_r\tan\alpha \tag{3}$$

$$l_{ext} = n\overline{A_iD_i} + (n+1)\overline{A_iD_{i+1}} + c_r = n(p - 2w_r\tan\alpha) + 2(n+1)\frac{w_r}{\cos\alpha}\sin\left(\alpha + \frac{\sigma}{2}\right) + c_r \tag{4}$$

$$l_{int} = n\overline{A_iD_i} + (n+1)\overline{B_iC_{i+1}} + c_r = n(p - 2w_r\tan\alpha) + 2(n+1)\frac{w_r}{\cos\alpha}\sin\left(\alpha - \frac{\sigma}{2}\right) + c_r \tag{5}$$

In equations (1)–(5), the constant geometrical parameters p (the vertebral pitch), w_r, and α characterize the geometry of the vertebrae, while the variable angle σ is the angular displacement of each vertebral joint; the angle σ is limited by the geometry of the plates between 0 and 2α.

When the vertebral column is rectilinear, σ is null and:

$$l_{ext} = l_{int} = np + 2w_r\tan\alpha + c_r = l_{med} \tag{6}$$

Consequently, the variations of the lengths of the external rope (positive) and of the internal rope (negative) are, respectively, as follows:

$$\Delta l_{ext} = l_{ext} - l_{med} = 2(n+1)w_r\left(\frac{\sin(\alpha + \sigma/2)}{\cos\alpha} - \tan\alpha\right) \tag{7}$$

$$\Delta l_{int} = l_{int} - l_{med} = 2(n+1)w_r\left(\frac{\sin(\alpha - \sigma/2)}{\cos\alpha} - \tan\alpha\right) \tag{8}$$
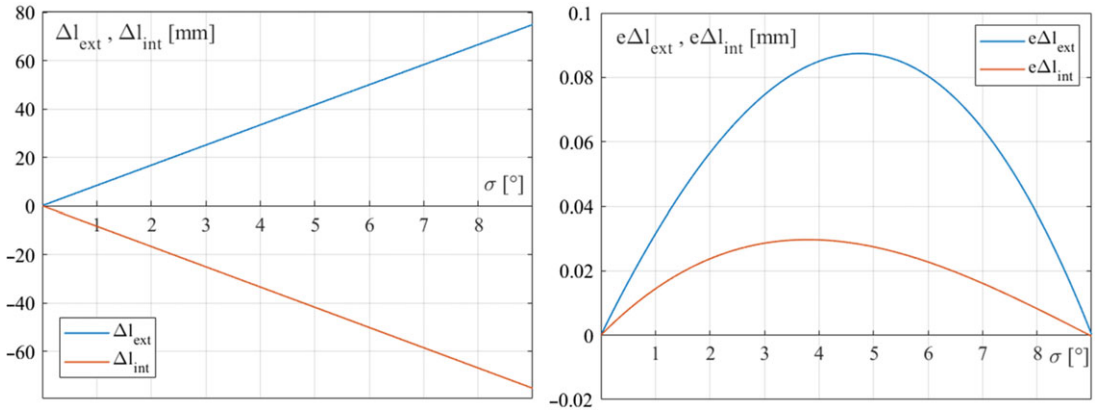
Figure 8. *Variations of the rope lengths as functions of the yaw angle of the vertebral joints (left); differences between the variations of the rope lengths and their linear approximations as functions of the yaw angle of the vertebral joints (right).*

For the Porcospino prototype, $n = 10$, $p = 40$ mm, $w_r = 43.5$ mm, and $\alpha = 4.5°$. Figure 8 (left) shows the graphs of Δl_{ext} and Δl_{int} as functions of σ with these parameters.

It is possible to notice that:

- the maximum magnitudes are similar but not perfectly equal: $\Delta l_{ext,max} = 74.8$ mm, $\Delta l_{int,min} = 75.3$ mm;
- the relationships are almost linear.

In order to evaluate the linearity of the equations (7) and (8), Fig. 8 (right) shows the differences $e\Delta l_{ext}(\sigma)$ and $e\Delta l_{int}(\sigma)$ between $\Delta l_{ext}(\sigma)$ and $\Delta l_{int}(\sigma)$ and their linear approximations passing through the end points at $\sigma = 0$ and $\sigma = 2\alpha$.

It is possible to note that these differences are negligible (the maximum values are, respectively, 0.09 mm for $e\Delta l_{ext}$ and 0.03 mm for $e\Delta l_{int}$); consequently, it is evident that for real-time control purposes, and it is adequate to use the linear approximations.

Considering the geometry of Fig. 7 (right), it is possible to observe that the center of the circular trajectory of the vertebral column is the intersection of the transversal axes of the vertebrae (dash-dotted in Fig. 7). This allows to calculate the turning radius r_t of the vertebral column as a function of σ:

$$r_t = \frac{p}{2 \tan\left(\frac{\sigma}{2}\right)} \tag{9}$$

Figure 9 (left) shows the turning radius r_t and its inverse, the curvature $\kappa_t = 1/r_t$, as a function of σ. For $\sigma = 0$, the column is rectilinear, r_t tends to infinity, and κ_t is null; for $\sigma = 2\alpha$, the turning radius is minimum (254 mm) and the curvature is maximum (3.93×10^{-3} 1/mm).

The kinematics expressed by equations (7)–(9) has been experimentally validated by comparing the relationship between the internal rope displacement $\Delta l_{int,min}$, which drives the steering motion, and the corresponding curvature α_t, obtained analytically and experimentally. The analytical relationship can be obtained by means of equations (8) and (9):

$$\kappa_t = \frac{2}{p} \tan\left(\alpha - \arcsin\left(\left(\tan\alpha + \frac{\Delta l_{int}}{2(n+1)\,w_r}\right)\cos\alpha\right)\right) \tag{10}$$

In Fig. 9 (right), the blue graph represents equation (10), while the green markers indicate the experimental measures. The orange dotted horizontal line represents the maximum curvature (3.93×10^{-3} 1/mm). It is possible to note that the real rope displacement is slightly higher than the
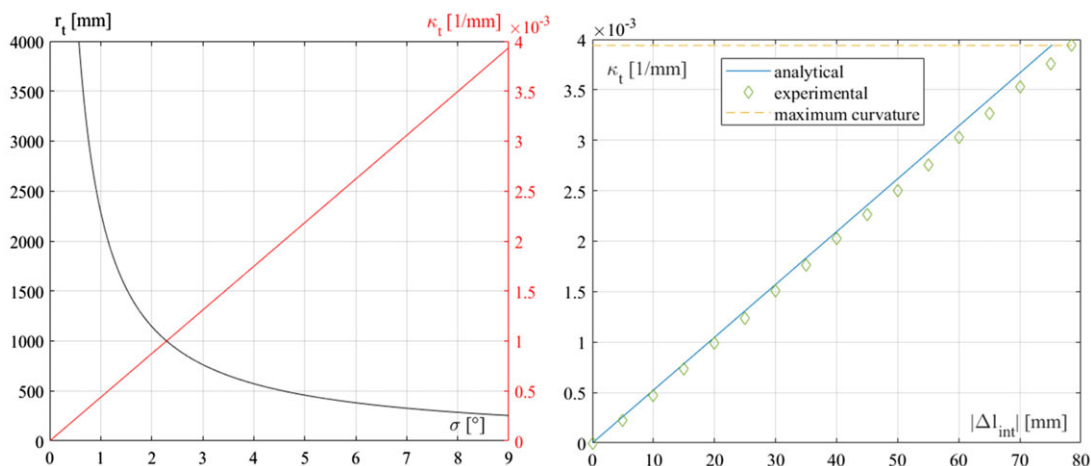
Figure 9. *Turning radius r_t and curvature κ_t of the vertebral column as a function of the yaw angle of the vertebral joints (left); curvature κ_t as a function of Δl_{int} (right).*

corresponding analytical value for any curvature due to the elasticity of the rope and to the approximations in the geometry of Fig. 7: in the prototype, the hole edges in the vertebral modules are slightly rounded to reduce rope friction and wear. In the real system, the maximum curvature is obtained for $\Delta l_{int} = 78.5$ mm, instead of the theoretical value of 75.3 mm. The experimental results confirm that the linear approximation of the steering kinematics is suitable for navigation purposes, since the difference between the linear and nonlinear relationships (Fig. 8, right) is much lower than the approximation introduced by the elasticity of the real system.

6. Prototyping and experimental tests

The first Porcospino prototype, realized for the preliminary experimental campaign, is manually radio-controlled by an operator. The tests have confirmed the feasibility and functionality of the proposed single-track architecture, and its capability of steering exploiting the active lateral flexion of the vertebral column and of adapting to ground irregularities, thanks to the passive retroflexion and torsion of the vertebral column, improving traction.

The following tests have been carried out:

- locomotion on different types of flat surfaces (compact, grassy, and gravelly) to validate the steering effectiveness and maneuverability (Fig. 10 and 11);
- locomotion on uneven grounds (Figs. 12 and 13);
- climbing of square steps (Fig. 14);
- locomotion on soft terrains (Fig. 15, left);
- experiments of pipe inspection (Fig. 15, right);
- recovery maneuvers after capsizing on a flank (Fig. 16).

A video about the experimental campaign is available in ref. [30].

The frame sequence of Fig. 10 shows Porcospino moving on a flat and compact indoor ground, showing the functionality of the steering system: the robot switches from rectilinear configuration (first frame, $t = 0.0$ s) to its minimum turning radius (fourth and fifth frames, $t = 3.1 \div 4.0$ s). Figure 11 shows a similar maneuverability test performed on an outdoor terrain, partially grassy and partially gravelly, but quite compact; also in this case, the steering system is capable of changing effectively the curvature of the
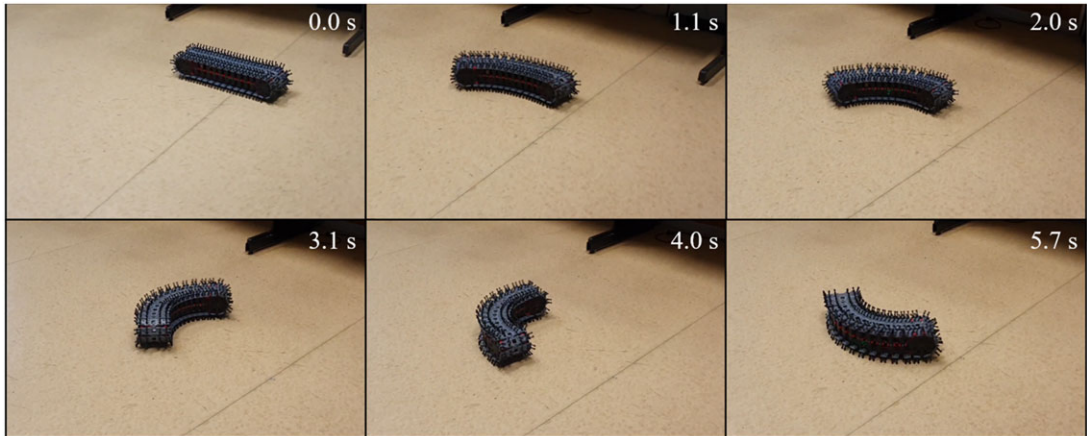
Figure 10. *Maneuverability tests on flat and compact ground: the robot switches from rectilinear configuration (0.0 s) to maximum curvature (3.1–4.0 s).*
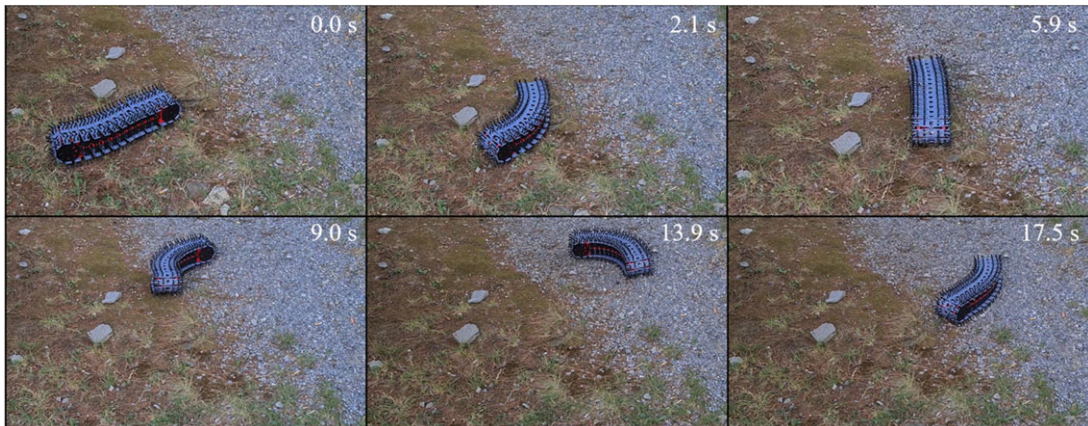

Figure 11. *Maneuverability tests on grassy and gravelly flat terrain.*

vertebral column. In Fig. 11, the third frame ($t = 5.9$ s) shows an intermediate position while switching curvature direction: the vertebral column is not perfectly aligned, since it is underactuated, as discussed in Section 4, and its dynamic behavior is influenced by the interactions with the ground irregularities.

The frame sequences of Figs. 12 and 13 show the passive adaptability of the vertebral column on terrain irregularities. In particular, in the motion of Fig. 12, the retroflexion is mainly exploited, while in the motion of Fig. 13, both retroflexion and torsion are performed.

While the tracks equipped with elastic spines of Porcospino offer indeed a much better traction and shock absorption on compact grounds, as in the tests of Figs. 12 and 13, in case of tall grass, leafy, or sandy terrains, the spines can get caught, limiting the robot mobility. In these cases, the robot can be equipped with a track without elastic spines, similarly to the SnakeTrack, to increase the contact surface and to reduce sinkage on yielding grounds. However, if the height of grass and foliage is lower than $30 \div 40$ mm, as in most operative conditions for the target applications, the spined track does not limit the mobility (Fig. 15, left).

The frame sequence of Fig. 14 represents Porcospino climbing a square step, showing the effectiveness of the elastic spines in grasping the step edge to lift the robot front; in this figure, the step height is 73 mm, which corresponds to 50% of the track height. The height of the maximum climbable step
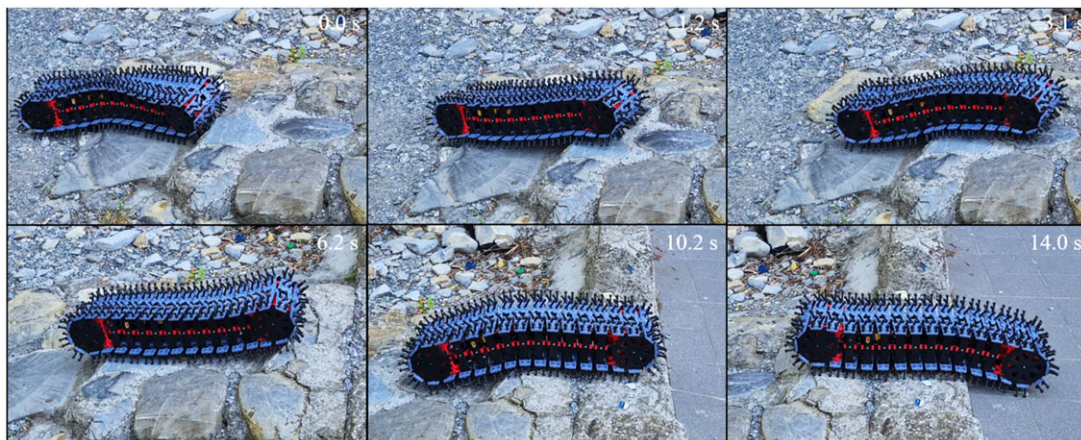
Figure 12. *Experimental tests: passive adaptability of the vertebral column on terrain irregularities (retroflexion).*
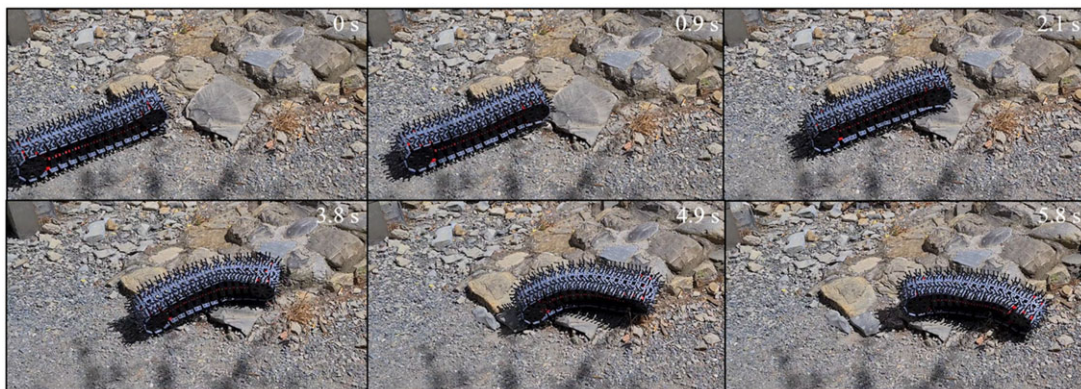

Figure 13. *Experimental tests: passive adaptability of the vertebral column on terrain irregularities (retroflexion and torsion).*

is difficult to be quantified exactly since it depends on the friction conditions, both without the spines (SnakeTrack) or with the spines (Porcospino); however, the ratio between the maximum climbable step and the robot height increases by 12–15% adopting the spines, as measured experimentally comparing the two prototypes while climbing square steps of different materials (wood, stone, plastic). Figure 15 (right) shows the inspection of a pipe with 300 mm diameter. In the case of pipe inspection, the rows of elastic spines mounted on the track edges bend, thus increasing the adherence to the pipe cylindrical surface.

An important issue for mobile robots moving in unstructured environments is tip-over. Some researchers try to prevent tip-over through proper motion planning [31]; a different and intrinsically safer way is to design robots that can recover operativity after a tip-over [13]. Porcospino follows this second approach. The frame sequence of Fig. 16 shows the capability of recovering a correct locomotion position after a 90° capsize on a flank. The maneuver is performed by curving the vertebral column through the steering actuators, until the robot reaches an unstable position, suspended on its ends (fourth frame, $t = 3.2$ s); then, a small motion of the tracks causes the fall on the correct locomotion position (fifth frame, $t = 3.7$ s). The same maneuver is shown in the video available in ref. [30]; at $t = 1:18$ s, it is possible to observe that after the bump, the robot bounces due to the compliance provided by the
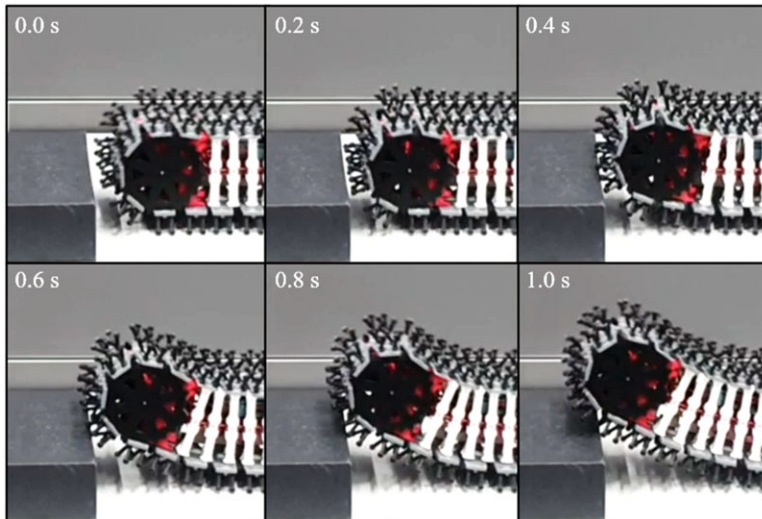
Figure 14. *Experimental tests: climbing of a square step, detail of the elastic spines grasping the step edge to lift the robot front.*

Figure 15. *Experimental tests: locomotion on grassy and leafy soft terrain (left) and inspection of a pipe with diameter of 300 mm (right).*

elastic spines, indicating the effectiveness of the shock adsorption. A deeper investigation of the influence of the spine stiffness on shock adsorption and step climbing performance will be addressed in future works.

Overall, the experimental campaign has shown the functionality of the Porcospino concept, even if refinements of the detailed design are necessary to further increase the reliability of the track guiding system. With respect to the first prototype, the SnakeTrack, without spines on the tracks [21], the experimental tests have shown the effectiveness of the spines to improve traction on irregularities in the presence of firm ground, and a certain degree of shock absorption. Nevertheless, spines are counterproductive on soft and yielding terrains, since they reduce the contact surface with the ground. However, the robot concept is fully modular, and not only the robot length can be varied based on the specific task but also the track type.
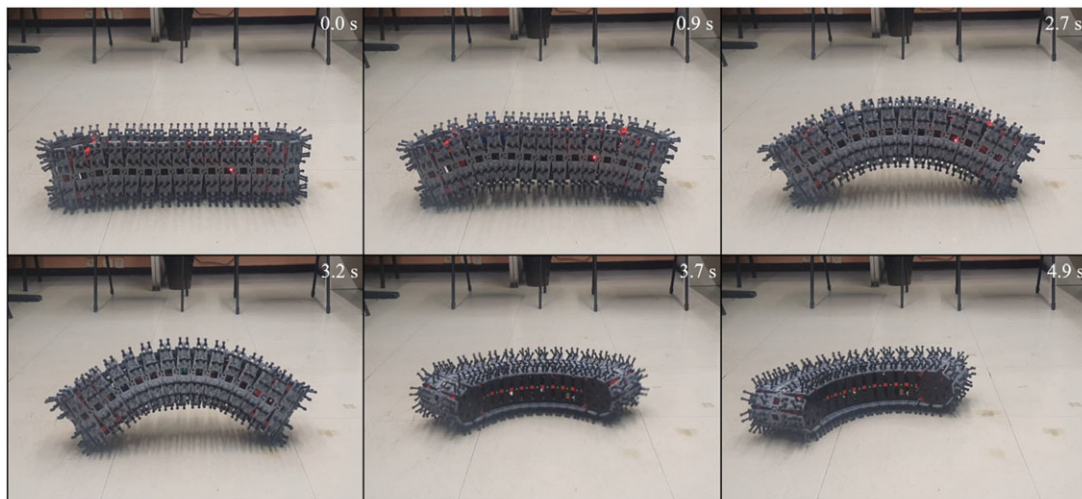
Figure 16. Experimental tests: recovery maneuver after a capsize on a flank.

7. Conclusions and future developments

The mechanical design of Porcospino, a small-size single-track robot for surveillance and inspection of unstructured and narrow spaces, has been presented. The functional design of the robot, the embodiment design of the vertebral joints, and the kinematics of the cable-driven steering maneuver have been discussed.

The active lateral flexion of the vertebral column can be used to steer, while passive retroflexion and torsion allow to cope with terrain irregularities. The Porcospino structure is fully modular, and its length can be varied to host sensors required for the specific mission.

Thanks to its small turning radius (254 mm), its maneuverability in narrow spaces is good. It cannot pivot around a vertical axis as differential steering robots, but this is not a remarkable limitation, due to the full bidirectionality.

The symmetry of Porcospino brings another useful functional feature: it can continue operating after a 180° capsize; moreover, if it falls on a flank (90° capsize), it can use active lateral flexion and track motion to restore its operativity.

Porcospino is the second version of a family of single-track steering robots; the main difference with respect to its predecessor, SnakeTrack, is the presence of flexible spines on the track modules, which are particularly effective to improve traction on uneven but firm terrains. Moreover, they introduce a certain degree of shock absorption, which increases the overall structural survivability of the robot. Other improvements are refinements of the shape of the track guidance system (lateral supports, LS, Fig. 5, and guiding pegs, GP, Fig. 3). As a matter of fact, the track guidance system is the main weak point of the concept, and further work must be done to reach a degree of reliability sufficient for real applications.

Provided that these issues are solved, and a proper technology readiness level is obtained, the proposed design seems to be interesting for inspection of narrow unstructured environments, such as pipelines or collapsed buildings, thanks to its small front section and adaptability to unevenness.

In the future of work, another important topic to be addressed is the development of an active retroflection system to increase the obstacle climbing capability.

Competing interests. The authors declare no conflicts of interest exists.

Ethical approval. Not applicable.

References

[1] A. Mahapatra, S. S. Roy and D. K. Pratihar, "Multi-legged Robots – A Review," **In:** *Multi-body Dynamic Modeling of Multi-legged Robots* (Springer, Singapore, 2020) pp. 11–32.

[2] S. Rodinò, E. M. Curcio, A. Di Bella, M. Persampieri, M. Funaro and G. Carbone, "Design, simulation, and preliminary validation of a four-legged robot," *Machines* **8**(4), 82 (2020).

[3] R. E. Arvidson, K. D. Iagnemma, M. Maimone, A. A. Fraeman, F. Zhou, M. C. Heverly, P. Bellutta, D. Rubin, N. T. Stein, J. P. Grotzinger and A. R. Vasavada, "Mars science laboratory curiosity rover megaripple crossings up to Sol 710 in Gale crater," *J. Field Robot.* **34**(3), 495–518 (2017).

[4] G. Colucci, L. Tagliavini, A. Botta, L. Baglieri and G. Quaglia, "Decoupled motion planning of a mobile manipulator for precision agriculture," *Robotica*, **98**(1), (2023).

[5] G. Ottonello, G. Berselli, L. Bruzzone and P. Fanghella, "Functional Design of Elloboat, a Tracked Vehicle for Launching and Beaching of Watercrafts and Small Boats," **In:** *Proc. of the 2018 14th IEEE/ASME International Conference on Mechatronic and Embedded Systems and Applications, MESA 2018*, Oulu, Finland (2018) pp. 1–8.

[6] W. Tao, Y. Ou and H. Feng, "Research on dynamics and stability in the stairs-climbing of a tracked mobile robot," *Int. J. Adv. Robot. Syst.* **9**(4), 146 (2012).

[7] P. Ben-Tzvi, A. A. Goldenberg and J. W. Zu, "Design, Simulations and Optimization of a Tracked Mobile Robot Manipulator with Hybrid Locomotion and Manipulation Capabilities," **In:** *Proc. of the 2008 IEEE International Conference on Robotics and Automation*, Pasadena, CA, USA (2008) pp. 2307–2312.

[8] S. Hirose, Y. Fukuda, K. Yoneda, A. Nagakubo, H. Tsukagoshi, K. Arikawa, G. Endo, T. Doi and R. Hodoshima, "Quadruped walking robots at Tokyo Institute of Technology," *IEEE Robot. Autom. Mag.* **16**(2), 104–114 (2009).

[9] I. Moskvin, R. Lavrenov, E. Magid and M. Svinin, "Modelling a Crawler Robot Using Wheels as Pseudo-Tracks: Model Complexity vs Performance," **In:** *Proc. of the 7th IEEE International Conference on Industrial Engineering and Applications (ICIEA 2020)*, Bangkok, Thailand (2020) pp. 1–5.

[10] X. Gao, D. Cui, W. Guo, Y. Mu and B. Li, "Dynamics and stability analysis on stairs climbing of wheel-track mobile robot," *Int. J. Adv. Robot. Syst.* **14**(4), 1–13 (2017).

[11] G. Quaglia, L. G. Butera, E. Chiapello and L. Bruzzone, "UGV epi.q-mod," **In:** *Proc. 20th CISM-IFToMM Symposium on Theory and Practice of Robots and Manipulators, ROMANSY 2014*, Mechanisms and Machine Science, vol. **22**, Moscow, Russia (2014) pp. 331–339.

[12] K. Tadakuma, R. Tadakuma, A. Maruyama, E. Rohmer, K. Nagatani, K. Yoshida, A. Ming, M. Shimojo, M. Higashimori and M. Kaneko, "Mechanical Design of the Wheel-Leg Hybrid Mobile Robot to Realize a Large Wheel Diameter," **In:** *Proc. of the IEEE/RSJ International Conference on Intelligent Robots and Systems*, Taipei, Taiwan (2010) pp. 3358–3365.

[13] L. Bruzzone, M. Baggetta, S. E. Nodehi, P. Bilancia and P. Fanghella, "Functional design of a hybrid leg-wheel-track ground mobile robot," *Machines* **9**(1), 1–11 (2021).

[14] L. Bruzzone and G. Quaglia, "Review article: Locomotion systems for ground mobile robots in unstructured environments," *Mech. Sci.* **3**(2), 49–62 (2012).

[15] M. Neumann, T. Predki, L. Heckes and P. Labenda, "Snakelike, tracked, mobile robot with active flippers for urban search-and-rescue tasks," *Ind. Robot* **40**(3), 246–250 (2013).

[16] N. Li, S. Ma, M. Wang, B. Li and Y. Wang, "An Optimization Design Method for the Mechanism Parameters of an Amphibious Transformable Robot," **In:** *Proc. 2012 IEEE/RSJ International Conference on Intelligent Robots and Systems*, Vilamoura, Portugal (2012) pp. 2282–2288.

[17] L. Bruzzone, S. E. Nodehi and P. Fanghella, "Tracked locomotion systems for ground mobile robots: A review," *Machines* **10**(8), 648 (2022).

[18] T. Kinugasa, T. Haji, K. Yoshida, H. Amano and K. Osuka, "Lateral Movement of Flexible Mono-tread Mobile Track (FMT) - Modeling, Simulation and Experiment," **In:** *Proc. of the 2009 International Conference on Advanced Robotics (ICAR2009)*, Munich, Germany (2009) pp. 1–6.

[19] T. Haji, T. Kinugasa and K. Yoshida, "Experiment of maneuverability of flexible mono-tread mobile track and differential-type tracked vehicle," *Ind. Robot* **37**(3), 263–272 (2010).

[20] T. Kislassi and D. Zarrouk, "A minimally actuated reconfigurable continuous track robot," *IEEE Robot. Autom. Lett.* **5**(2), 652–659 (2020).

[21] S. E. Nodehi, L. Bruzzone and P. Fanghella, "SnakeTrack, a Bio-Inspired, Single Track Mobile Robot with Compliant Vertebral Column for Surveillance and Inspection," **In:** *Proc. of the 31st International Conference on Robotics in Alpe-Adria-Danube Region, RAAD 2022*, Mechanisms and Machine Science, vol. **120 MMS**, Klagenfurt, Austria (2022) pp. 513–520.

[22] L. Tamas, G. Lazea, M. Popa, I. Szoke and A. Majdik, "Laser and vision based object detection for mobile robots," *Int. J. Mech. Control* **11**(1), 89–95 (2010).

[23] G. Reina, N. I. Giannoccaro, A. Messina and A. Gentile, "A 3D-laser scanner for autonomous mobile robots," *Int. J. Mech. Control* **11**(1), 21–27 (2010).

[24] G. Balakrishnan and S. S. Hiremath, "Autonomous sensor networks for monitoring industrial processes with application to mobile robots," *Int. J. Mech. Control* **12**(1), 113–123 (2011).

[25] F. Crenna, G. B. Rossi and L. Bovio, "Probabilistic measurement evaluation for the implementation of the Measuring Instrument Directive," *Measurement* **42**(10), 1552–1531 (2009).

[26] D. F. Machekposhti, N. Tolou and J. L. Herder, "A review on compliant joints and rigid-body constant velocity universal joints toward the design of compliant homokinetic couplings," *J. Mech. Des.* **137**(3), 032301 (2015).

[27] L. Bruzzone and R. M. Molfino, "A novel parallel robot for current microassembly applications," *Assem. Autom.* **26**(4), 299–306 (2006).

[28] L. Bruzzone and G. Bozzini, "A flexible joints microassembly robot with metamorphic gripper," *Assem. Autom.* **30**(3), 240–247 (2010).

[29] P. Bilancia and G. Berselli, "An overview of procedures and tools for designing nonstandard beam-based compliant mechanisms," *Comput. Aided Des.* **134**(6), 103001 (2021).

[30] Porcospino, Spined Single-Track Mobile Robot for Inspection of Narrow Spaces (2023). https://youtu.be/pMXYwr75jq0

[31] M. Oehler, S. Kohlbrecher and O. Von Stryk, "Optimization-based planning for autonomous traversal of obstacles with mobile ground robots," *Int. J. Mech. Control* **21**(1), 33–40 (2020).